Green Chemistry

PAPER

View Article Online
View Journal | View Issue

Ab initio and classical simulations of the temperature dependence of zeolite pore sizes†

Cite this: *Green Chem.*, 2014, **16**, 875

Hongbo Shi,[a] Angela N. Migues[b] and Scott M. Auerbach*[a,b]

Ab initio and classical simulations were used to study the equilibrium and fluctuating ring diameters for all-silica zeolites SOD, FER, and MFI over the temperature range 300–900 K. Such simulations are important for understanding and predicting zeolite/guest fit, especially for relatively bulky guest species, *e.g.*, those derived from biomass. We simulated equilibrium zeolite structures, IR spectra, thermal expansion coefficients, and ring breathing vibrations to investigate the competition between negative thermal expansion and enhanced vibrational amplitudes with increasing temperature. We find that although negative thermal expansion tends to shrink equilibrium ring sizes with increasing temperature, this trend is nullified by considering ring breathing vibrations, giving effective pore sizes that are roughly constant with temperature, and larger than those extracted from X-ray data. Several force fields were tested and a modified BKS force field was found to give the best agreement with the simulated properties listed above, especially for MFI. Our results are consistent with previous work suggesting that effective zeolite ring sizes are underestimated by using oxygen ionic radii for estimating atomic excluded volume.

Received 17th August 2013,
Accepted 18th December 2013

DOI: 10.1039/c3gc41681j

www.rsc.org/greenchem

1. Introduction

The regular arrays of pores and channels in zeolites[1] make them indispensable tools for myriad green chemistry applications requiring shape-selective catalysts and adsorbents.[2] Zeolites may also provide efficient routes for producing fuels and chemicals directly from plant biomass,[3] thus being doubly green in terms of both process and feedstock. To achieve this important goal, we need better understanding of the role of zeolite flexibility[4] in processing biomass-derived species. On the one hand, zeolites are often thought of as highly incompressible solids with large bulk moduli in the range 10–100 GPa. On the other hand, zeolites can often adsorb and/or produce guest molecules with kinetic diameters larger than nominal zeolite pore sizes. For example, catalytic fast pyrolysis (CFP) studies of cellulose in contact with HZSM-5 zeolite at 600 °C carried out by Jae *et al.*[5] establish the production of naphthalene (~6.2 Å) in the channels of HZSM-5 (5.3 Å × 5.7 Å).[6] This raises the fundamental question of whether our conceptions of zeolite pore size – determined by X-ray data corrected by estimates of atomic radii – are useful for predicting zeolite/guest fit over a range of conditions (*e.g.*, at the high temperatures of CFP). Accurate pore-size estimates are crucial for designing selective zeolite-based separations and zeolite-catalyzed reactions – staples of green chemistry – with tight-fitting molecular substrates. To address this issue, we report the application of *ab initio* and classical molecular simulations in the present article to investigate the temperature dependences of pore sizes in small- and medium-pore zeolite types SOD, FER, and MFI.

It is not obvious a priori how heating zeolites influences their effective pore sizes. Indeed, the behaviour of zeolites with increasing temperature likely involves the competition between negative thermal expansion which decreases average pore sizes;[7] and enhanced thermal vibrations of pores and channels,[4] which serve to increase effective pore sizes. This competition may be better understood by positing a hierarchy of zeolite structure/energy fluctuations. Towards this end for a given zeolite, we denote the zeolite framework potential energy fluctuation $\Delta V = V(\boldsymbol{r}) - V(\boldsymbol{r}_0)$, where $V(\boldsymbol{r})$ is the zeolite potential energy at the framework structure given by $\boldsymbol{r}$, and $V(\boldsymbol{r}_0)$ is the ground state potential energy at the optimal (low pressure) geometry $\boldsymbol{r}_0$. [In what follows we ignore the quantity $V_0 = V(\boldsymbol{r}_0)$, which sets the zero of energy but often has little additional physical meaning except in the case of ionic models, for which $|V_0|$ is the vaporization energy of an ionic solid to its corresponding plasma, which itself has little relevance for the present discussion.]

The hierarchy of zeolite structure/energy fluctuations can be understood with the following Taylor-series expansion:

$$\Delta V = \Delta V_1 + \Delta V_2 + \Delta V_3, \quad (1)$$

where ΔV_1 arises from linear displacements, ΔV_2 is the quadratic potential, and ΔV_3 provides cubic corrections. The

[a]Department of Chemical Engineering, University of Massachusetts, Amherst, MA 01003, USA. E-mail: auerbach@chem.umass.edu
[b]Department of Chemistry, University of Massachusetts, Amherst, MA 01003, USA
†Electronic supplementary information (ESI) available. See DOI: 10.1039/c3gc41681j

expansion in eqn (1) maps onto the following hierarchy of length scales for a given zeolite pore:

$$d^{\mathrm{eff}}(T) = d_1 + \Delta d_2(T) + \Delta d_3(T), \quad (2)$$

where d_1 is an optimized equilibrium pore size obtained when $\Delta V_1 = 0$, $\Delta d_2(T)$ arises from thermal vibrations at fixed-volume controlled by the quadratic term ΔV_2,[8] and $\Delta d_3(T)$ is from thermal expansion or contraction controlled by the cubic correction Δd_3.[9] This hierarchy relies on the fact that harmonic oscillators do not exhibit thermal expansion/contraction; anharmonicities such as cubic terms are required to produce such phenomena.[10]

Zeolite pore sizes are usually estimated by measuring d_1 with low- and/or room-temperature X-ray diffraction (XRD), and subtracting a correction for oxygen excluded volume, typically (but not always[5]) using oxygen's crystal ionic radii 1.35 Å.[11] However, relatively few systematic studies have been reported[4] on the temperature dependences of thermal vibrations ($\Delta d_2(T)$) and thermal expansion/contraction ($\Delta d_3(T)$), and how these influence effective pore sizes. Thermal expansion/contraction (*i.e.*, $\Delta d_3(T)$) can be measured by high-temperature XRD,[7,12] but $\Delta d_2(T)$ is harder to probe experimentally.[4] Several groups have sought to understand zeolite flexibility at fixed-volume (*i.e.*, $\Delta d_2(T)$) by measuring and modelling infrared (IR) spectra of zeolite frameworks.[13–15] However, we argue below that IR spectra may focus on vibrations that are not directly relevant to zeolite pore size. Because of the difficulty in fully understanding zeolite pore sizes by experiments alone, we have engaged in *ab initio* and classical simulations (informed by some experimental data) to shed light on these issues.

Because the quantities d_1 and $\Delta d_3(T)$ can be measured by XRD, we lump them together into an effective quantity $d(T) = d_1 + \Delta d_3(T)$. We expect $d(T)$ to be a decreasing function of temperature because of the well-established phenomenon of zeolite thermal contraction.[7] For the sake of understanding zeolite/guest fit, we estimate the quantity $\Delta d_2(T)$ as the standard deviation of fluctuating ring diameters obtained during our simulations, denoted as $\sigma(T)$. This is motivated by the idea that the *outer turning point* of a ring breathing vibration provides a better estimate of effective pore size than does the equilibrium pore size given by $d(T)$. We expect $\sigma(T)$ to increase with temperature because harmonic vibrational amplitudes scale as the square root of temperature. To test these predictions, we apply simulations to compute $d(T)$ and $\sigma(T)$ to determine how these quantities vary with temperature for all-silica zeolites SOD, FER, and MFI.

Most simulations of zeolite framework flexibility have relied on classical, force field models of the potential energy. Such force fields are often fitted to select experimental data such as low-temperature XRD patterns or IR spectra. However, it is clear from the above discussion that, for the present study, we would require a force field that reproduces all of the following data: low-temperature XRD, high-temperature XRD, and vibrational spectra such as Raman or inelastic-neutron spectra of zeolites. Few if any force fields have been fitted to such an array of data. In the absence of such a force field, we turn to *ab initio* molecular dynamics (MD) simulations such as the Car-Parrinello MD (CPMD) approach[16] to provide accurate simulation data on zeolite framework fluctuations. Ab initio MD has been used to understand many reactions in zeolites,[17–19] and the corresponding plane-wave density functional theory (DFT) has shed light on many structural and mechanical properties of zeolite solids.[9,10] Below we show that *ab initio* simulation provides a powerful tool for understanding pore size fluctuations in SOD, FER, and even in the larger MFI structure.

Despite the importance of *ab initio* MD, force fields will likely be the method of choice for simulating zeolites and zeolite framework fluctuations for the foreseeable future. As such, we do seek a force field that can capture as much of the physics behind eqn (1) and (2) as possible. For example, Smirnov *et al.*[20,21] reported a computational study of ring fluctuations with a force field that reproduces zeolite structure (d_1) and vibrational frequencies (related to $\Delta d_2(T)$), but they did not demonstrate the capability of this force field for modelling thermal expansion/contraction ($\Delta d_3(T)$). On the other hand, the force field used by Yamahara[22] reproduces the thermal contraction of MFI, but the predicted vibrational spectrum in the low-frequency region which may be important for pore breathing vibrations was not shown. Below we report a slightly modified version of the force field developed by van Beest, Kramer and van Santen[23] that simultaneously reproduces key aspects of zeolite structure (especially for MFI), ring-breathing amplitudes predicted by CPMD, and negative thermal expansion coefficients measured experimentally.

The findings described below can facilitate the design and optimization of zeolite-based separations and zeolite-catalyzed reactions. For example, sustainable production of *para*-xylene, a key precursor for making plastics and fibers, through cycloaddition of substituted furan and olefins has recently been demonstrated in the large-pore zeolite HY.[24] Our findings below may suggest whether running the process in a medium-pore zeolite such as HZSM-5 may enhance the *para*-xylene yield. Other green-chemistry processes such as zeolite-catalyzed fast pyrolysis of biomass to biofuels[25] and microwave-heated, catalytic conversion of cellulose to intermediate chemicals in zeolites[26] may also be optimized with proper estimates of zeolite pore size.

The remainder of this paper is organized as follows: in section 2 we describe the *ab initio* and classical simulation methods, and also the physical properties calculated; in section 3 we report and discuss the *ab initio* simulation results, and then the classical simulation data including those from the modified force field; and in section 4 we offer concluding remarks.

2. Methodology

A. Zeolite systems

X-ray crystallographic data for all-silica zeolites SOD,[27] FER,[27] and MFI[28] provided initial atomic coordinates for

Table 1 Unit cell parameters and repetitions in the simulation boxes

	Unit cell parameters			Simulation box	
Zeolite type	*a* (Å)	*b* (Å)	*c* (Å)	CPMD	Classical
SOD	8.96	8.96	8.96	1 × 1 × 1	2 × 2 × 2
FER	19.01	14.30	7.54	1 × 1 × 1	1 × 1 × 2
MFI	20.02	19.89	13.38	1 × 1 × 1	1 × 1 × 2

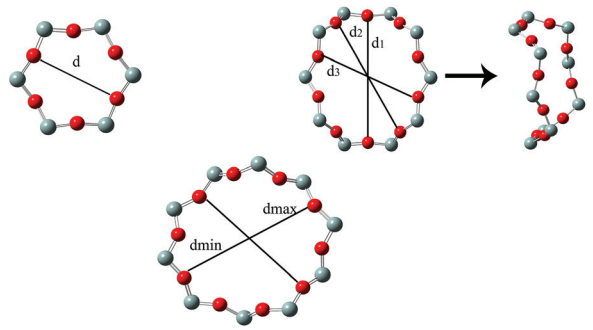

Fig. 1 Rings in SOD (top left), FER (top right), and MFI (bottom).

optimizations and molecular dynamics simulations (MD). The orthorhombic MFI structure of van Koningsveld *et al.*,[28] stable at temperatures above ~350 K, was studied because of our primary interest in high-temperature framework dynamics. The lattice parameters and system sizes for *ab initio* and classical simulations are listed in Table 1, which shows the larger systems sizes considered by our classical simulations.

Periodic boundary conditions were applied to all simulation cells, effectively surrounding the system with infinite mirror images to approximate macroscopic crystals.

Tight-fitting guest diffusion in zeolites is typically controlled by the largest rings that form connected windows and channels in a given zeolite structure. Thus in this work we considered ring sizes for rings with the largest diameters. The relevant rings of SOD, FER, and MFI are shown in Fig. 1. Ring diameters always refer herein to the distances between opposing oxygen atoms. Ring sizes are labeled by the number of alternating Si–O moieties; *e.g.*, a ring with 6 alternating Si–O linkages is called a "6-ring." The three possible diameters of the 6-rings of SOD are equal by symmetry (Fig. 1); small thermal fluctuations that deviate from such SOD symmetry are ignored below. The 10-ring window in all-silica FER zeolite deviates strongly from planarity. Due to symmetry, three distinct diameters are observed in a single 10-ring of FER. The 10-ring in MFI is elliptical; we focus on the maximum and minimum diameters.

B. *Ab initio* simulations

Ab initio optimizations and molecular dynamics simulations were performed using the Car-Parrinello MD (CPMD) software package, which has been successfully applied to investigate the structural and electronic properties of zeolites.[29] In this

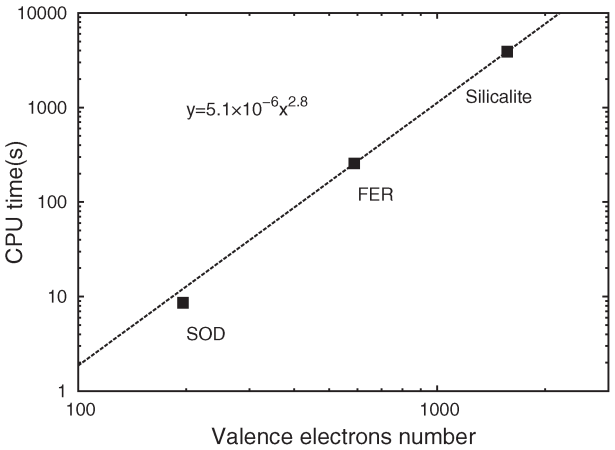

Fig. 2 CPU time (per processor per dynamic step) scaling with system size expressed as the number of valence electrons.

work, the local density approximation (LDA) has been used for the exchange-correlation potential; we have shown in earlier work that LDA does a surprisingly good job of reproducing zeolite unit cell volumes and mechanical properties, in many cases better than gradient-corrected functionals.[9] Filippo[29] has also shown that in strongly bonded systems such as zeolites, LDA performs well in describing the structures. To solve the uniform homogeneous electron gas problem, we used the Teter–Pade parameterization. Vanderbilt ultrasoft pseudopotentials were used to represent core-valence electronic interactions for both silicon and oxygen atoms. Valence electrons were represented explicitly using plane waves with a 30 Ry cutoff for all the systems studied below. Because of system size constraints, the Brillouin zone was sampled with Γ-point sampling in all cases.[9]

Single-point wave function calculations were used to begin both geometry optimizations and MD simulations. The electron fictitious mass in dynamics was set to 400 au to ensure good adiabatic behavior of electronic dynamics.[30] In constant temperature dynamics, both ions and electrons were thermostatted by Nosé–Hoover chains.[31–33] Target temperatures for electron kinetic energies were obtained by running short (~1 ps) simulations in which only ion temperatures were thermostatted; the resulting average fictitious electron kinetic energies were taken as the targets for subsequent electron temperature control. The time step for moving atoms was set to 4 au and trajectories were written to disk every 33 steps.

Fig. 2 shows that the CPU time required for each CPMD step scales with the number of electrons to the power 2.8 for the three zeolites studied herein. More details on the system sizes and CPU times can be found in the ESI.† *Ab initio* dynamics for SOD and FER were performed for 30 ps. Because of the great expense of CPMD applied to the MFI zeolite structure, dynamics were run only at the 300 K case for 2 ps.

C. Classical modeling

Classical molecular simulations compute interparticle interactions through empirical force fields parameterized by either

experimental properties and/or first principle calculations. Since there is no need to calculate electronic distributions, CPU times are significantly reduced and larger system sizes can be treated. However, classical simulation results depend largely on the force field parameters used. The transferability and accuracy of force fields are limited because most force fields are generated by reproducing a limited set of properties. Despite these limitations, we seek below a single force field that can reasonably reproduce zeolite structures, vibrations, and thermal expansion properties for the SOD, FER, and MFI frameworks.

We mainly compared three different types of force field. The force field developed by Auerbach *et al.*[34] contains Buckingham potentials (eqn (3)), Columbic potentials, and three-body potentials. The three body term accounts for the relative rigidity of SiO_4 tetrahedra. For simplicity this force field will be referred to as "Three Body Force Field" (TBFF). Three body potentials in DL_POLY have a different form (eqn (4)), requiring us to refit the TBFF to this form.

$$V^{\text{short}}_{\text{Buckingham}} = A\exp\left(\frac{-r}{\rho}\right) - \frac{C}{r^6}, \tag{3}$$

$$V^{\text{tbp}}_{\text{Harmonic}} = \frac{k}{2}(\theta-\theta_0)^2\exp\left(\frac{-r_{ij}^8 - r_{jk}^8}{\rho^8}\right), \tag{4}$$

We also considered the Beest, Kramer, and van Santen force field[35] (BKSFF), fitted to *ab initio* data and containing the same potential terms as TBFF except that BKSFF lacks three-body potential terms. BKSFF has been shown to reproduce elastic constants and negative thermal expansion for CHA and SAS zeolites.

We also considered the force field developed by Pedone, Malavasi, Menziani, Cormack, and Segre[36] (PMMFF), which includes the Morse potential for the short-range interaction. Like the BKSFF, the PMMFF lacks three body potential terms. PMMFF is able to reproduce structural parameters and mechanical properties of a wide range of crystalline silicates. The force field developed by Yamahara *et al.*[22] (YOKFF), and a modified version of the BKSFF (MBKSFF) were also considered. All force field parameters used in this study are given in the ESI.†

For our classical simulations, we used the parallel DL_POLY-2 package which was developed at Daresbury Laboratory.[37] We have performed constant volume (NVT) classical molecular dynamics with target temperature of 300 K, 600 K and 900 K. The data collected during these simulations were used to compute equilibrium structure, infrared spectrum and ring distributions. At each temperature, the experimental volume[12,38,39] was used, thus the effect of thermal contraction was included. The temperature was controlled during the simulation by Nose-hover thermostat[31–33] with relaxation time of 0.1 ps. To calculate the equilibrium volume and thermal expansion coefficients, constant pressure (NPT) simulations were performed. Pressure and temperature were controlled by Berendsen thermostat with relaxation time of 0.1 ps. The initial configurations for all dynamics at higher temperatures were obtained by isotropic decrease of that in 300 K. Initial velocities were randomly assigned by Maxwell Boltzmann distribution. We used the leap frog algorithm[40] to integrate Newton's equation with a time step of 1 fs. For electrostatic interactions, we used Ewald summations with a cutoff smaller than the half of the minimum cell vector length. Trajectories were stored for 100 ps and written to disk every 4 steps.

D. Structure optimization

Structure is a primary property in PES evaluation. We optimized the structures of SOD, FER and MFI by both an initio and classical simulations. In *ab initio* simulations the minimum energy configurations were searched using the conjugate gradient method with a max force threshold value of 10^{-3} au. In addition the geometries were also optimized with DL_POLY, implemented by a combination of conjugate gradient and low temperature dynamics, using a threshold value of 10^{-5} au.

The atom positions in the relaxed structure are recorded and the average standard deviations, R^{opt}, from the experimental structures are calculated according to:

$$R^{\text{opt}} = \sqrt{\frac{1}{N}\sum_i^N (\boldsymbol{r}^{\text{opt}} - \boldsymbol{r}^{\text{exp}})^2}, \tag{5}$$

where $\boldsymbol{r}$ is the atom coordinates and N is the total number of particles in the simulation systems.

E. Equilibrium structure

The experimental structures that we used for comparison were extracted from the X-ray crystallographic data. The measured atomic coordinates correspond to the equilibrium geometry on the PES. Thus a more accurate comparison would be provided if dynamics were used to determine the equilibrium structure through averaging of the atom positions.

In CPMD simulations for SOD, a center of mass shift was observed. In order to compare the SOD structures the resultant movement of the center of mass was deducted. The structural deviation, R^{eq}, at 300 K was calculated according to

$$R^{\text{eq}} = \sqrt{\frac{1}{N}\sum_i^N (\langle \boldsymbol{r}_i^{\text{eq}}\rangle - \boldsymbol{r}_i^{\text{exp}})^2}, \tag{6}$$

where r_i^{eq} is the ensemble average of ith atom's coordinates.

F. Infrared spectrum

Vibrational frequencies are usually measured by infrared (IR) spectroscopy and are dependent on the second derivatives of the PES. The simulation method would be more reliable if the calculated computed IR peaks are in close agreement with experimental results.

Typically the IR spectrum calculation utilizes linear response theory through a Fourier transform of the total dipole moment auto correlation function as follows:[41,42]

$$I(\omega)_{\text{cl}} = \frac{1}{2\pi}\int_{-\infty}^{+\infty} \mathrm{d}t e^{-\mathrm{i}\omega t}\left\{\langle \vec{\boldsymbol{M}}(t)\cdot\vec{\boldsymbol{M}}(0)\rangle - |\langle\vec{\boldsymbol{M}}\rangle|^2\right\}, \tag{7}$$

where $I(\omega)_{cl}$ is the spectral density or the classical absorption lineshape, and ω is the angular frequency. In classical modeling, the dipole moment at each step is calculated according to:

$$\boldsymbol{M}(t) = \sum_{i}^{N} q_i \boldsymbol{r}_i(t), \quad (8)$$

where q and $\boldsymbol{r}$ represent the charge and the coordinates associated with ith atom. The IR spectrum can be obtained using atomic velocities and charges.[42] This approach avoids discontinuities in atomic positions that arise when employing periodic boundary conditions.[43] The intensities obtained by this method are qualitative because the quantum corrections needed to give completely accurate intensities are impractical for such a large system.[44] Previous MD trajectories were used to calculated IR intensities.

G. Thermal expansion coefficient

Thermal expansion coefficients were calculated for the total volume at 200 K–900 K. In CPMD NPT simulations, the volume exhibited a physically meaningless periodic oscillation. As such the algorithm in CPMD NPT is not applicable to thermal expansion coefficients and classical NPT simulation was used to determine this property.

Linear regression analysis was performed and the slopes were used to calculate thermal expansion coefficients according to:

$$\alpha_V = \frac{1}{V(300\ \mathrm{K})}\frac{dV}{dT}, \quad (9)$$

H. Ring distribution

Average ring diameters and standard deviations were calculated at 300 K, 600 K, and 900 K. To obtain better statistics, the ring diameters were averaged over time and the simulation box through:

$$d = \frac{\sum_{k=1}^{N_{ring}}\sum_{j=1}^{N_{sym}}\sum_{i=1}^{N_{step}} d_{ijk}}{N_{ring} \times N_{sym} \times N_{step}}, \quad (10)$$

where N_{step} represents the number of dynamic simulation steps, N_{sym} is the number of symmetric diameters in the same ring. N_{sym} is 3 for SOD and 2 for d_2 in FER (Fig. 1). N_{ring} is the number of similar rings in the simulation box. For example, we used four 10-rings to sample d_{min} and d_{max}.

Standard deviation of each distance σ_{jk} was first calculated over time using eqn (11) and then σ was calculated by average over the simulation box.

$$\sigma_{jk} = \sqrt{\frac{\sum_{i=1}^{N_{step}} (d_i - < d >)^2}{N_{step}}}, \quad (11)$$

where < > is the ensemble average.

3. Results and discussion

Here we report our *ab initio* simulation results for the equilibrium structures, IR spectra, and ring breathing vibrations in SOD, FER and MFI-type zeolites. We will then use the CPMD results, partnered with experimental data, to evaluate the applicability of different force fields for describing such properties.

A. Structures

Table 2 shows the simulated structural deviations, R^{opt} and R^{eq}, determined using both CPMD and classical dynamics. The structures of SOD and FER obtained from *ab initio* simulations agree reasonably well with experimental data with a standard deviation, R^{eq}, of <0.1 Å. In the case of MFI, the R^{eq} is greater than 0.1 Å but still relatively small at 0.18 Å. Longer simulation times may be necessary to decrease the R^{eq} of MFI but at this time are not computationally tractable. In general the small deviations between the *ab initio* simulation and the experimental structure prove that *ab initio* simulation is both a reliable and accurate tool for modeling zeolite structure.

We have also used classical simulation and employed different force fields to determine the deviations in all three zeolites (see Table 2). Although BKSFF and PMMFF are slightly better than TBFF at modeling the structure of SOD and FER, the deviations in MFI by these two Force fields are much greater due to large distortions in the framework. These results confirm that force field simulations are highly dependent on the potential forms and parameters used in their development and as such lack the universal applicability and transferability of *ab initio* simulations. Without further refinement, BKSFF and PMMFF are not good candidates for describing the structural properties of MFI, such as ring distribution. Based on BKSFF, we increased the point charges of Si and O in MFI and obtained a modified BKSFF (MBKSFF, see Table S2†), which reproduces an equilibrium MFI structure closest to experiments among all the force fields used in this study.

B. Infrared spectrum at 300 K

The infrared spectra for SOD and FER at 300 K are shown in ESI (Fig. S1†). Several studies[21,45,46] have suggested peak assignments in the lower wavenumber region (400–750 cm^{-1}) to ring vibrations. Analysis for isolated rings[47] of silico-oxygen tetrahedra has shown that a single band located in the region

Table 2 Deviation of optimized structure R^{opt} and equilibrium structure R^{eq} from experiment

Potential	SOD		FER		MFI	
	R^{opt} (Å)	R^{eq} (Å)	R^{opt} (Å)	R^{eq} (Å)	R^{opt} (Å)	R^{eq} (Å)
CPMD	0.08	0.04	0.02	0.05	0.03	0.18
TBFF	0.07	0.08	0.10	0.07	0.13	0.14
BKSFF	0.02	0.07	0.07	0.05	0.57	0.60
PMMFF	0.02	0.06	0.05	0.06	0.57	0.59
YOKFF	0.06	0.12	0.04	0.12	0.43	0.35
MBKSFF	0.07	0.04	0.08	0.08	0.20	0.12

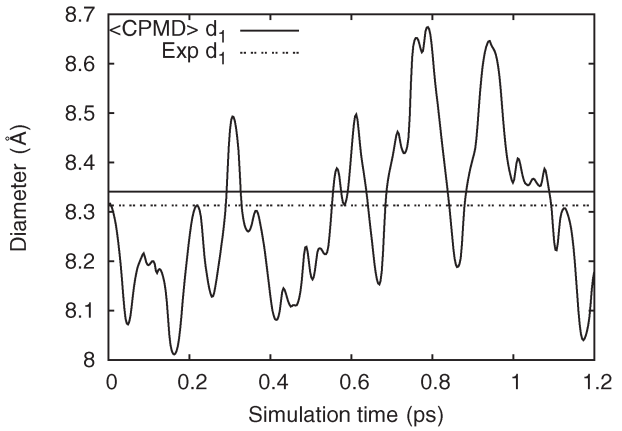

Fig. 3 Ring diameter d_1 evolves with time for FER by CPMD at 300 K. Experimental d_1 is from XRD measurement.[27]

of the so-called pseudolattice vibrations (400–800 cm^{-1}) corresponds to the ring vibration. Increasing the size of the ring results in the shift of characteristic band positions toward lower wavenumbers.[48] This suggests that vibrational frequencies for even larger rings such as 10-rings may fall below the typical infrared wavenumber window for zeolites (400–1200 cm^{-1}).[48] Fig. 3 shows the ring diameter oscillation for FER obtained from CPMD simulation. The frequency of the ring diameter vibration can be roughly estimated by counting the number of waves per picosecond and was determined to be around 200 cm^{-1}. Another method to calculate the frequency is to perform a Fourier transform of the ring diameter auto correlation function over a short time-scale (0.2 ps). This method produced a broad frequency distribution ranging from 0–400 cm^{-1} with a notable peak at 120 cm^{-1}. Therefore the peak in IR spectrum for FER at approximately 400 cm^{-1} should not be assigned to ring vibration. The infrared spectrum is thus not an effective property to evaluate the applicability of force fields for modeling ring vibrations in medium to large pore zeolites. As such we conclude that CPMD is a better suited method for studying the direct ring vibrations in zeolites.

C. Thermal contraction at standard pressure

Negative thermal expansion (NTE) in zeolites has been observed experimentally in many zeolites such as siliceous Sodalite,[49] LTA,[50] MFI,[12] ITQ-7 and ITQ-9.[51] In order to reproduce NTE behavior accurately, the force field used should include the anharmonic contributions of the PES, as close to that of the true PES.[10] In NPT dynamic simulations using TBFF, the unit cell tends to quickly shrink followed by subsequent collapse. This suggests that either the TBFF calculation is not stable with respect to this algorithm or that the TBFF constructed PES deviates too much from the true PES at large displacements. Fig. 4 shows the volume change with respect to temperature for 200 K–900 K. The experimental data used for comparing, SOD, FER and MFI were taken from Zheng,[38] Bull[39] and Bhange[12] respectively. The thermal expansion coefficients determined by all force fields agree reasonably well with experimental results (Table 3). However, PMMFF and BKSFF tends to overestimate the volume which agrees with the results of previous simulations by Combariza[23] regarding Si-CHA and Si-SAS. Unit cell volume calculated by modified BKSFF is very close to the experiment value for all three zeolites in a wide range of temperature. In Fig. 4, a maximum point for FER was observed in the experimental data at 400 K. We have not been able to simulate this phenomenon with any of the force fields studied, however since our simulations focus on higher temperature regimes it is not necessary to reproduce.

D. Ring distribution at 300, 600 and 900 K

As shown above, CPMD provides a practical way to obtain ring size distributions. Fig. 5 shows fluctuations of d_1 in two different 10-rings in the FER simulation box. A timescale of 30 ps was sufficient to minimize statistical error in the fluctuation calculation. However simulating the fluctuations in MFI on such a time-scale is not computationally tractable due to a significant increase in system size compared to FER. Fig. 5 also suggests that at 2 ps, the fluctuations in FER fall into the region where statistical error is 10%.

Thus we assume that a 2 ps time-scale for simulation of MFI is sufficient to model ring fluctuation within 10% uncertainty. Although there is more error associated with a shorter time-scale, understanding the dynamics in MFI will provide some information for the vibration.

Average ring diameters and fluctuations for SOD and FER are plotted in Fig. 6. Simulations for the two zeolites show similar trends with respect to temperature dependent ring distributions. We conclude the following from Fig. 6:

1. In SOD the contribution of σ to d^{eff} is ~0.4 Å, almost 15% of the 'static' ring size (2.6 Å using standard atomic radii). This suggests that ring vibration needs to be considered in catalysis design, especially for tight-fitting guest molecules.

2. The average ring size d decreases when the temperature increases, indicating that the bridging oxygen atoms tend to explore the space inside the pores, which might responsible for the NTE phenomenon.

3. The ring fluctuation amplitude σ is much bigger than the average ring size change from one temperature to the next $[\Delta d = d(T_2) - d(T_1)]$. This suggests that it may be more important to model the ring vibrations than the contraction properties.

4. The effective ring diameter $d + \sigma$ appears roughly independent of temperature.

Fig. 7 and 8 show the FFs calculation for ring size distribution of SOD and FER. All FFs show good agreement with *ab initio* simulations in structure calculation in a wide temperature range; however, the fluctuations of SOD rings predicted by YOKFF is closer with *ab initio* results. For FER, PMMFF shows excellent agreement with *ab initio* simulations results in ring fluctuation calculations.

We find from Fig. S1† that the IR spectra predicted by all the force fields overestimate the frequencies in the lower

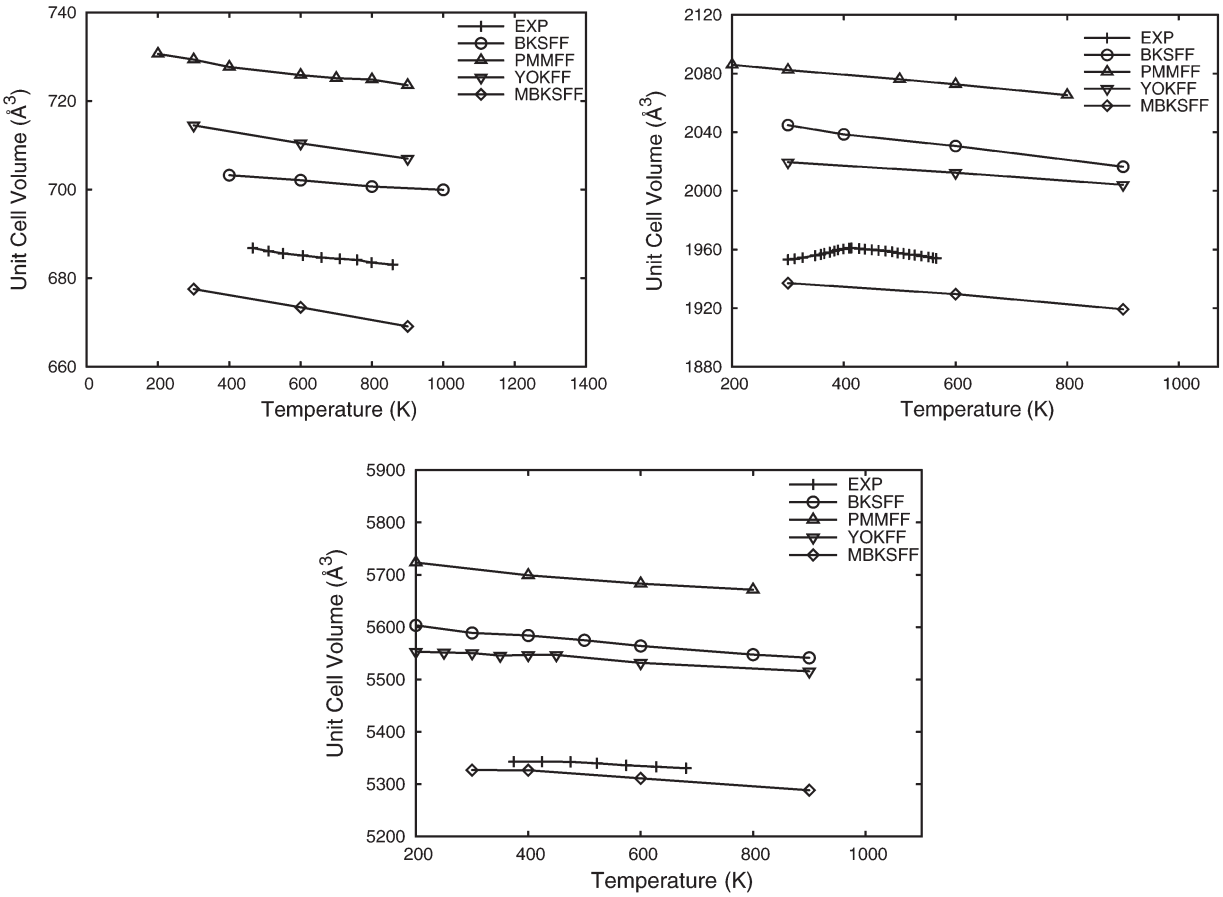

Fig. 4 Unit cell volume calculated by FFs for SOD (top left), FER (top right) and MFI (bottom). Experimental data are from ref. 38, 39 and 12.

Table 3 Thermal expansion coefficient

	$\alpha_V \times 10^6$ (K^{-1})		
	SOD	FER	MFI
EXP	−13.0[a]	−24.2[39]	−7.6[12]
BKSFF	−8.0	−22.5	−16.6
PMMFF	−13.3	−16.3	−15.6
YOK	−17.5	−12.7	−10.0
MBKSFF	−20.7	−12.5	−12.7

[a] Calculated based on volume data[38] by eqn (9).

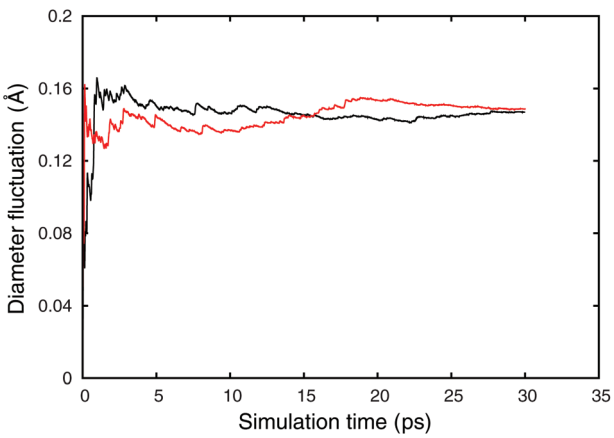

Fig. 5 Ring diameter fluctuations evolve with time for FER by *ab initio* dynamics; two lines represent the diameter of same type (d_1) but in different rings of in simulation box.

wavenumber region. According to eqn (S4),† ring vibration amplitudes should be underestimated using all three force fields if lower frequency region accounts for ring vibrations, which however is not the case. On the other hand, PMMFF shows highest discrepancy in all frequency regions simulation for FER, but closest to *ab initio* simulation results in ring fluctuation calculations. These results again suggest that the peaks at approximately 400 cm^{-1} should not be assigned to ring vibration and infrared spectrum is not an effective property to evaluate the applicability of force fields for modeling ring vibration.

Due to the limitation of current computer capability, it is unlikely to get accurate ring distribution for MFI using *ab initio* dynamics. The only information we may extract from previous 2 ps NVT dynamics for MFI is an estimation of 10-rings vibration amplitude (Table 4) with 10% error. Using ionic radius of 1.35 Å[11], d_{max}^{eff} of MFI becomes 5.92 ± 0.2 Å, still

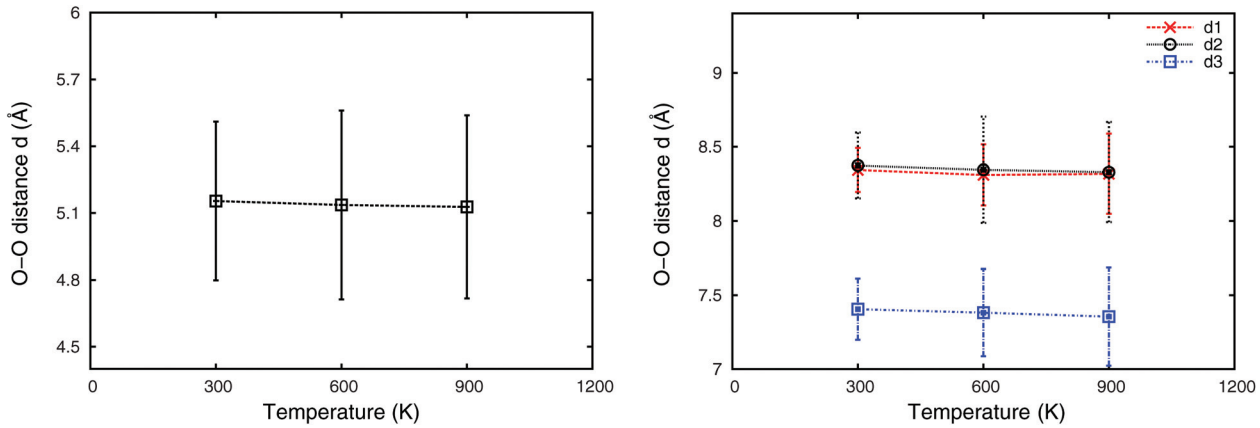

Fig. 6 SOD and FER ring distributions by CPMD at 300 K, 600 K and 900 K; error bar represents standard deviation σ.

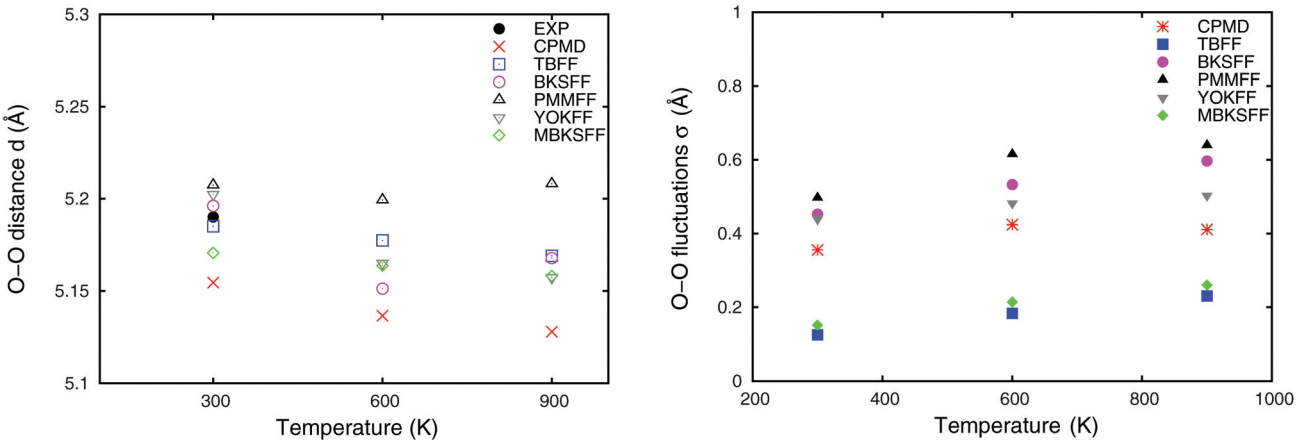

Fig. 7 Comparison of FFs dynamics with CPMD in SOD ring distributions at 300 K, 600 K and 900 K.

smaller than naphthalene kinetic diameter. Thus, in addition to the flexibility of the ring size, a proper choice for the atomic size should be considered to explain the anomalous host–guest fitting phenomenon.[52]

To evaluate the force fields ability to accurately model zeolite structure we compare ring sizes. Table 4 shows the maximum and minimum equilibrium ring sizes in MFI 10-rings. *Ab initio* dynamics again shows high accuracy in structure calculation. The ring shape determined by BKSFF and PMMFF is much more elliptical than that reported experimentally, which explains the high simulation deviation for structures in Table 2. MBKSFF shows best performance in the static ring modeling.

Ab initio calculation suggests that MFI has a larger ring than SOD and FER but a smaller fluctuation. The framework environment where the ring is located should highly affect the ring motions. The fluctuations of the maximum and minimum rings are also shown. All FFs shows similar capability in modeling the fluctuation amplitude for MFI.

Among the force fields, MBKSFF shows best performance in structure, ring size, ring fluctuation and thermal contraction calculation for MFI at 300 K, thus a good candidate for classical modeling of MFI.

NVT dynamics with MBKSFF was carried out for 100 ps at 300 K, 600 K, and 900 K; average and fluctuation of d_{min} and d_{max} were then calculated and shown in Fig. 9. The opposite change of d_{min} and d_{max} indicates a less elliptical ring at higher temperature. d_{max}^{eff} is almost independent with the temperature, which indicates that molecules which cannot go into MFI channel at 300 K would also be rejected at 900 K.

4. Conclusions

We performed *ab initio* calculation for SOD, FER and MFI using geometry optimization and dynamics techniques. LDA functional shows high accuracy in calculating structure properties and were found better than BLYP functional for in IR computations. Ring distributions study for SOD and FER by *ab initio* dynamics shows that at elevated temperature the ring size d decreases, ring vibration amplitude σ increases and the

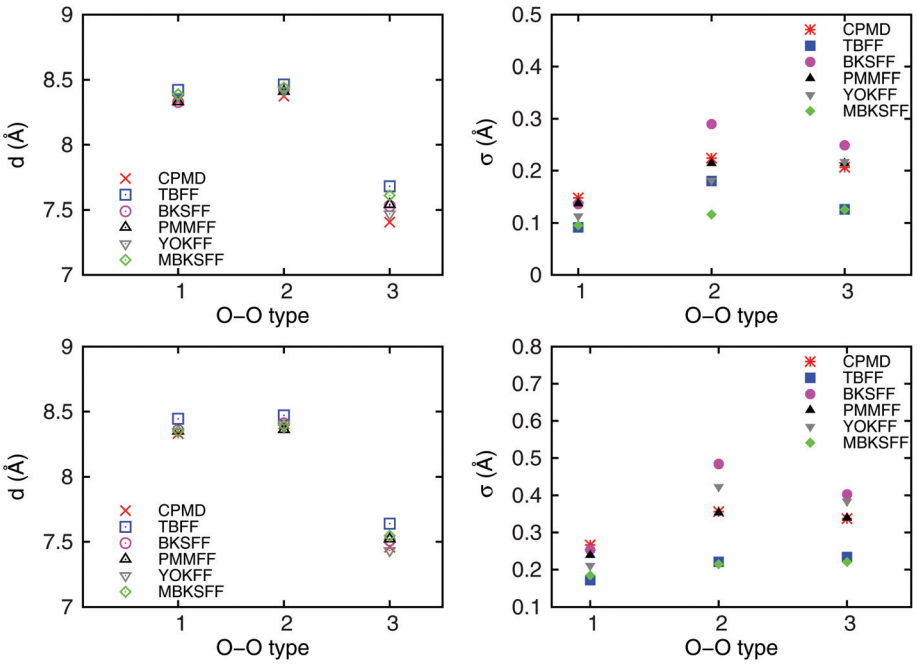

Fig. 8 Comparison of FFs dynamics with CPMD in FER Ring distributions at 300 K (top) and 900 K (bottom).

Table 4 Ring size data for MFI at 300 K

	d_{min} (Å)	d_{max} (Å)	σ (Å)
EXP[a]	7.92	8.45	N/A
CPMD	8.03	8.48	0.17
TBFF	8.32	8.39	0.2
BKSFF	7.13	9.53	0.19
PMMFF	7.11	9.56	0.17
YOKFF	7.41	9.26	0.2
MBKSFF	7.99	8.66	0.19

[a] From van Koningsveld.[28]

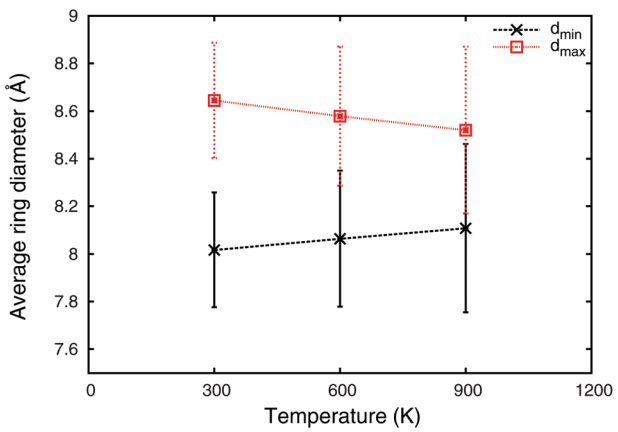

Fig. 9 MFI ring distributions at 300 K, 600 K, and 900 K by MBKSFF; error bar represents standard deviation σ.

effective ring diameters d^{eff} are approximately unchanged. We conclude that ring vibration should be considered in pore size calculation, especially for 6-ring in SOD.

Classical modelling was also performed using several force fields. Structure, vibration frequencies, thermal contraction and ring distributions was studied and the results were used for FFs evaluation. We find IR frequencies not important in ring motion simulations. YOKFF, PMMFF and MBKSFF are more accurate for modelling the structure and flexibility of SOD, FER and MFI respectively.

Classical modelling using the MBKSFF indicates that similar with SOD and FER, the effective value of the maximum ring diameter of the 10-rings in MFI the fluctuations of SOD rings MFI also shows no temperature dependence. In the future we will focus on framework-guest molecules interactions in tight-fitting host guest systems.

Acknowledgements

We thank Dr S. Vaitheeswaran and Jacob Harvey for simulation suggestions. We also thank Dr Andrew Teixeira for helpful discussions. This work was supported by the National Science Foundation (CBET 0932777).

References

1 S. M. Auerbach, K. A. Carrado and P. K. Dutta, *Handbook of Zeolite Science and Technology*, Marcel Dekker, New York, 2003.
2 A. Corma, *Chem. Rev.*, 1995, **95**, 559–614.
3 T. R. Carlson, J. Jae, Y. C. Lin, G. A. Tompsett and G. W. Huber, *J. Catal.*, 2010, **270**, 110–124.

4 M. W. Deem, J. M. Newsam and J. A. Creighton, *J. Am. Chem. Soc.*, 1992, **114**, 7198–7207.
5 J. Jae, G. A. Tompsett, A. J. Foster, K. D. Hammond, S. M. Auerbach, R. F. Lobo and G. W. Huber, *J. Catal.*, 2011, **279**, 257–268.
6 H. van Koningsveld, *Acta Crystallogr., Sect. B: Struct. Sci.*, 1990, **46**, 731–735.
7 D. S. Bhange and V. Ramaswamy, *Microporous Mesoporous Mater.*, 2007, **103**, 235–242.
8 S. C. Turaga and S. M. Auerbach, *J. Chem. Phys.*, 2003, **118**, 6512–6517.
9 R. Astala, S. M. Auerbach and P. A. Monson, *J. Phys. Chem. B*, 2004, **108**, 9208–9215.
10 R. Astala, S. M. Auerbach and P. A. Monson, *Phys. Rev. B: Condens. Matter*, 2005, **71**, 014112.
11 W. M. Meier, D. H. Olson and C. Baerlocher, *Zeolites*, 1996, **17**, 1–229.
12 D. S. Bhange and V. Ramaswamy, *Mater. Res. Bull.*, 2006, **41**, 1392–1402.
13 R. Bueno-Perez, S. Calero, D. Dubbeldam, C. O. Ania, J. B. Parra, A. P. Zaderenko and P. J. Merkling, *J. Phys. Chem. C*, 2012, **116**, 25797–25805.
14 K. S. Smirnov and D. Bougeard, *Catal. Today*, 2001, **70**, 243–253.
15 P. Bornhauser and D. Bougeard, *J. Phys. Chem. B*, 2001, **105**, 36–41.
16 R. Car and M. Parrinello, *Phys. Rev. Lett.*, 1985, **55**, 2471–2474.
17 C. Lo, C. A. Giurumescu, R. Radhakrishnan and B. L. Trout, *Mol. Phys.*, 2004, **102**, 281–288.
18 C. A. Giurumescu and B. L. Trout, *AIChE Symp. Ser.*, 2001, **97**, 313–316.
19 K. Schwarz, E. Nusterer and P. Margl, *Int. J. Quantum Chem.*, 1997, **61**, 369–380.
20 K. S. Smirnov and D. Bougeard, *J. Phys. Chem.-Us*, 1993, **97**, 9434–9440.
21 K. S. Smirnov and D. Bougeard, *J. Mol. Struct.*, 1995, **348**, 155–158.
22 K. Yamahara, K. Okazaki and K. Kawamura, *Catal. Today*, 1995, **23**, 397–402.
23 A. F. Combariza, G. Sastre and A. Corma, *J. Phys. Chem. C*, 2009, **113**, 11246–11253.
24 C. L. Williams, C. C. Chang, P. Do, N. Nikbin, S. Caratzoulas, D. G. Vlachos, R. F. Lobo, W. Fan and P. J. Dauenhauer, *ACS Catal.*, 2012, **2**, 935–939.
25 S. Vaitheeswaran, S. K. Green, P. Dauenhauer and S. M. Auerbach, *ACS Catal.*, 2013, **3**(9), 2012–2019.
26 J. González-Rivera, I. R. Galindo-Esquivel, M. Onor, E. Bramanti, I. Longo and C. Ferrari, *Green Chem.*, 2013, DOI: 10.1039/C3GC42207K.
27 C. Baerlocher and L. B. McCusker, Database of Zeolite Structures, http://www.iza-structure.org/databases/
28 H. van Koningsveld, H. van Bekkum and J. C. Jansen, *Acta Crystallogr., Sect. B: Struct. Sci.*, 1987, **43**, 127–132.
29 F. Filippone, F. Buda, S. Iarlori, G. Moretti and P. Porta, *J. Phys. Chem.-Us*, 1995, **99**, 12883–12891.
30 G. Pastore, E. Smargiassi and F. Buda, *Phys. Rev. A*, 1991, **44**, 6334.
31 S. Nosé, *Mol. Phys.*, 1984, **52**, 255.
32 W. Hoover, *Phys. Rev. A*, 1985, **31**, 1695.
33 P. H. Hünenberger, *Adv. Polym. Sci.*, 2005, **173**, 105.
34 S. M. Auerbach, N. J. Henson, A. K. Cheetham and H. I. Metiu, *J. Phys. Chem.-Us*, 1995, **99**, 10600–10608.
35 B. W. van Beest, G. J. Kramer and R. A. van Santen, *Phys. Rev. Lett.*, 1990, **64**, 1955–1958.
36 A. Pedone, G. Malavasi, M. C. Menziani, A. N. Cormack and U. Segre, *J. Phys. Chem. B*, 2006, **110**, 11780–11795.
37 I. T. Todorov, W. Smith, K. Trachenko and M. T. Dove, *J. Mater. Chem.*, 2006, **16**, 1911–1918.
38 Z. K. Zheng, V. V. Guliants and S. Misture, *J. Porous Mater.*, 2009, **16**, 343–347.
39 I. Bull, P. Lightfoot, L. A. Villaescusa, L. M. Bull, R. K. B. Gover, J. S. O. Evans and R. E. Morris, *J. Am. Chem. Soc.*, 2003, **125**, 4342–4349.
40 D. Frenkel and B. Smit, *Understanding Molecular Simulation: From Algorithms to Applications*, 2002.
41 P. H. Berens and K. R. Wilson, *J. Chem. Phys.*, 1981, **74**, 4872–4882.
42 V. Agarwal, G. W. Huber, W. C. Conner and S. M. Auerbach, *J. Chem. Phys.*, 2011, **135**, 134506.
43 P. Bornhauser and D. Bougeard, *J. Raman Spectrosc.*, 2001, **32**, 279–285.
44 J. B. Nicholas, A. J. Hopfinger, F. R. Trouw and L. E. Iton, *J. Am. Chem. Soc.*, 1991, **113**, 4792–4800.
45 A. J. M. de Man and R. A. van Santen, *Zeolites*, 1992, **12**, 269–279.
46 W. Mozgawa, *J. Mol. Struct.*, 2001, **596**, 129–137.
47 M. Sitarz, W. Mozgawa and M. Handke, *J. Mol. Struct.*, 1997, **404**, 193–197.
48 M. Sitarz, M. Handke and W. Mozgawa, *Spectrochim. Acta, Part A*, 1999, **55**, 2831–2837.
49 L. Leardini, A. Martucci and G. Cruciani, *Microporous Mesoporous Mater.*, 2012, **151**, 163–171.
50 T. Carey, A. Corma, F. Rey, C. C. Tang, J. A. Hriljac and P. A. Anderson, *Chem. Commun.*, 2012, **48**, 5829–5831.
51 P. Lightfoot, D. A. Woodcock, M. J. Maple, L. A. Villaescusa and P. A. Wright, *J. Mater. Chem.*, 2001, **11**, 212–216.
52 M. Cook and W. C. Conner, in Proceedings of the International Zeolite Conference, 12th, Baltimore, 1998, p. 409.

